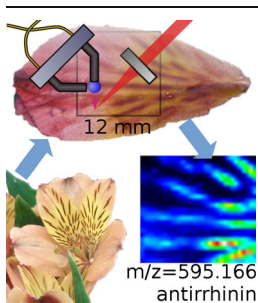RESEARCH ARTICLE

Mass Spectrometric Imaging Using Laser Ablation and Solvent Capture by Aspiration (LASCA)

Jonathan I. Brauer, Iwona B. Beech, Jan Sunner

Department of Microbiology and Plant Biology, University of Oklahoma, Norman, OK 73019, USA

Abstract. A novel interface for ambient, laser ablation-based mass spectrometric imaging (MSI) referred to as laser ablation and solvent capture by aspiration (LASCA) is presented and its performance demonstrated using selected, unaltered biological materials. LASCA employs a pulsed 2.94 μm laser beam for specimen ablation. Ablated materials in the laser plumes are collected on a hanging solvent droplet with electric field-enhanced trapping, followed by aspiration of droplets and remaining plume material in the form of a coarse aerosol into a collection capillary. The gas and liquid phases are subsequently separated in a 10 μL-volume separatory funnel, and the solution is analyzed with electrospray ionization in a high mass resolution Q-ToF mass spectrometer. The LASCA system separates the sampling and ionization steps in MSI and combines high efficiencies of laser plume sampling and of electrospray ionization (ESI) with high mass resolution MS. Up to 2000 different compounds are detected from a single ablation spot (pixel). Using the LASCA platform, rapid (6 s per pixel), high sensitivity, high mass-resolution ambient imaging of "as-received" biological material is achieved routinely and reproducibly.

Keywords: Laser ablation, Mass spectrometric imaging, Chemical imaging, Biological material, Sampling interface, Ambient mass spectrometry

Introduction

A variety of ambient mass spectrometric imaging (MSI) methods [1], in particular laser ablation (LA) based techniques, such as matrix-assisted laser desorption ionization (MALDI) [2], electrospray-assisted laser desorption/ionization (ELDI) [3], laser ablation electrospray ionization (LAESI) [4, 5], and matrix-assisted laser desorption electrospray ionization (MALDESI) [6, 7], have been developed in the past decade and applied to diverse biological systems. Although LA/MSI methods offer excellent control of sampled volumes, their possible limitations are low analyte collection and detection efficiencies. Moreover, the spatial resolution of LA/MSI methods is limited by the size of the laser focal area. With visible or UV laser light, a spot size close to 1 μm is achievable. However, for ambient imaging of biological materials, mid-IR lasers with a wavelength of 2.94 μm are commonly employed, as hydrated samples have

a relatively high extinction coefficient ($\approx 10^3$ cm^{-1}) at this wavelength because of strong absorption in water. Using a single focusing lens, the commonly used Nd:YAG/OPO lasers produce 2.94 μm laser light that has focal spot sizes with a practical minimum diameter of about 50 μm, mainly because of a relatively high laser beam divergence. Smaller spot sizes have been achieved through guiding the laser with a sharpened optical fiber [8].

Notwithstanding the importance of high spatial resolution, the practical usefulness of any MSI method for biological applications, in particular for statistical analysis of untargeted metabolomics data, is mainly governed by its ability to detect a large number of compounds in parallel in imaging mode. This is greatly facilitated by using a high-resolution mass spectrometer [9] with a wide dynamic range. This combination also enhances the capability to detect compounds that are relatively minor constituents of the metabolome, which is of critical importance for targeted metabolomics analysis. Since sample volumes analyzed in LA-MSI are generally small (a 50 μm spot size sampled to a depth of 10 μm equates to a 25 pLvolume), it is imperative to achieve the highest possible levels of analyte ionization and detection efficiencies. The importance of such developments is not limited to MSI. For example, the

Correspondence to: Jan Sunner; *e-mail:* Jan.Sunner-1@ou.edu

successful MS metabolomic analysis/imaging of a single bacterial cell would require that the combined sampling, ionization, and MS transmission efficiencies approach unity.

The major challenge for LA-MSI at atmospheric pressure is to achieve efficient sampling and ionization of analytes. An already demonstrated approach relies on entraining the ablation plume directly into an electrospray, as in ELDI [3] and related methods [4, 6, 7]. A range of different designs aid sampling of the ablated material directly into a liquid, usually followed by electrospray ionization of the solution. In its simplest implementation, the sampling surface can be that of a droplet suspended just above the ablation area [10–13]. The procedure is, however, slow; with robotic help, analysis of a single pixel can take 5 min [14], thus rendering it impractical for imaging purposes. An alternative to the capture of ablation products with a suspended droplet is to sample the plume directly into a flowing solvent stream. Such interfaces may have a coaxial [11, 13] or a linear geometry [15–18].

The trapping efficiency of laser-ablated analytes onto a droplet or a flowing solvent stream is generally low, at about 0.1%–1% [12, 15]. For low-fluence (<1 J/cm^2) mid-IR laser pulses, this is not surprising as the momentum of the plumes produced is small, and the plume penetration depth into atmospheric-pressure gas is only about 2–3 mm [19]. Furthermore, particles and molecules in the plume are small enough that they essentially follow laminar gas flow lines in front of an obstructing surface. Thus, their capture on the liquid surface is, presumably, limited by diffusion, which is a slow and inefficient process. Indeed, the "smoke" produced by a laser pulse can be observed to slowly drift away, following the ambient air movement. Clearly, there is a need for a more efficient method to entrain the ablation plume and its analytes into the liquid.

Previous reports demonstrated that the analyte sampling efficiency onto a liquid surface could be increased by up to two orders of magnitude by applying an electric field between the sample site and the collection surface [16, 17]. Since the analyte collection efficiency without an electric field is reported to be about 1% [15], the efficiency in the presence of an electric field is deduced to approach unity. It is noteworthy that a flowing solvent MS system is useful for imaging only if it is rapid (i.e., the time required to record the mass spectrum from a single pixel should be as short as possible), ideally not exceeding a few seconds. Recently, it was demonstrated that with a "liquid bridge" system [16], the abundances of ions formed from analytes ablated by a 1-s-long series of 20 laser pulses, increased rapidly for a few seconds. However, the decay time was much slower, with a half-life of about 10–20 s. Such a slow response not only increases the time required to record an image but also lowers the signal-to-noise ratios in the mass spectra, as a fixed amount of analyte is detected over a longer time period. Designing an interface with a faster response was, therefore, essential.

Here, we report the development of an LA-MS interface that uses a combination of aspiration and electrostatics to collect laser ablation plumes and that is capable of processing a pixel in 6 s or less. The method has been reported at conferences [20, 21] and its application to the characterization of biofilms on corroding metal surfaces has been demonstrated [22]. The Laser ablation and solvent capture by aspiration (LASCA) MSI system delivers high sensitivity, high spatial resolution images of large, rough biological specimens in as-received conditions (i.e., without the need for additional sample preparation). A fluid dynamics-based entrainment of the laser plume that separates the sampling and ionization processes is a key feature of the interface design. The ablated analytes from consecutive pixels are dissolved into a continuous solvent stream as analyte "plugs" (analogous to the output stream of a liquid chromatography system). The LASCA MSI system can be used with a variety of ionization techniques or with systems that collect the solvated analytes for later analysis (e.g., with NMR, PCR, or HPLC). Importantly, LASCA can be positioned independently some distance away from the MS ion source, without any modification to the commercial MS inlet. This allows large sample stages and, if required, environmental control of the imaging environment.

Methods

Laser System

A Nd:YAG-pumped, tunable OPO laser (IR Opolette 2731-HE; Opotek, Carlsbad, CA, USA) produces 4 ns, mid-IR laser pulses at a 20 Hz repetition frequency, and was tuned to 2.94 μm. The maximum pulse energy was 3.5 mJ, as measured using a pyroelectric energy meter (PE25-SH-V2; Ophir-Spiricon, Logan, UT, USA).

Sample Chamber and Stage

The imaging setup is shown schematically in Figure 1a. The experiment is performed in an airtight chamber that is pressurized with nitrogen gas to a pressure of 160 Torr above ambient pressure (A). The sample is placed on a 50 × 50 mm sample stage cooled by a Peltier cooling plate (TE-127-1.4-1.5; TE Technology, Traverse City, MI, USA) (B), which maintains the sample at temperatures down to –20° C. The heat generated from the Peltier element is transported out of the system with a water cooler and an external radiator. The sample stage is mounted on a motorized XYZ-stage (MTS50-Z8; Thorlabs, Newton, NJ, USA). The pulsed beam from the OPO laser (C) is directed by three gold mirrors (PF10-03-M01; Thorlabs) and enters the sample chamber through a quartz window (Technical Glass Products, Painesville, OH, USA). The beam is focused onto the sample surface by a 50-mm focal length CaF$_2$ spherical lens (CAPX11; Newport, Irvine, CA, USA). As the diameter of the incident beam is only 5 mm, the spherical aberration with this lens makes a negligible contribution to the focal spot size. The incidence angle on the sample is 60°; the size of the laser focus is 220 ± 10 μm $\times$ 260 ± 30 μm; and the pulse energy measured at the sample surface is 1.5 mJ. During imaging, the laser focal point remains fixed in space, while the sample is moved by the computer-controlled XYZ-stage. A binary
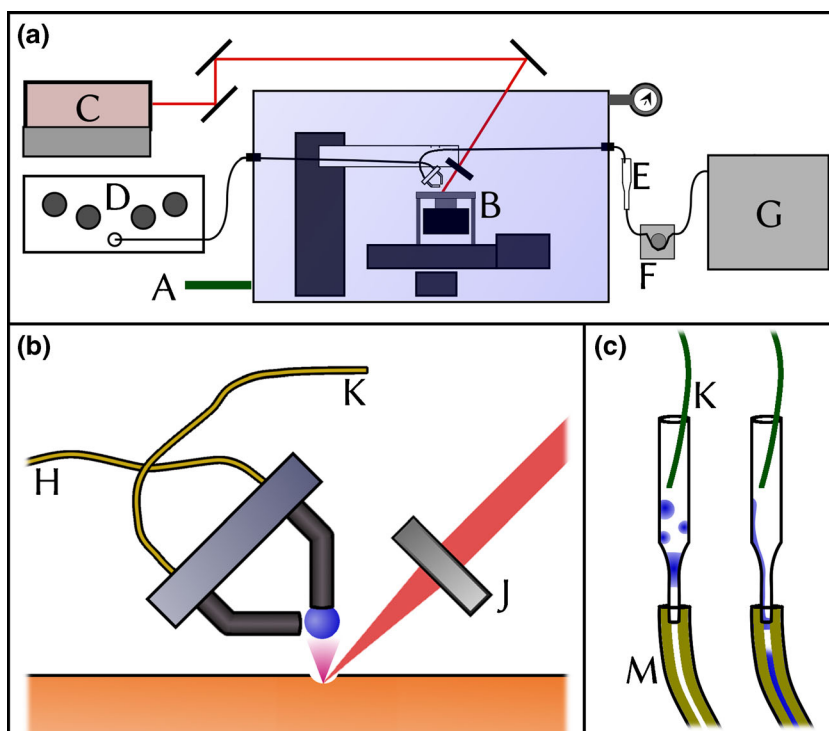
Figure 1. A schematic representation of LASCA imaging platform. Panel **(a)** depicts an overview of the system with: (A) the N_2 pressurized chamber (shaded blue) and (B) an X,Y-motorized and chilled specimen stage. The beam from an IR laser (C) is directed into the chamber and onto the specimen. Solvent is supplied to the collection interface with a HPLC binary pump (D), and the output flow is collected in a microfunnel (E) where nitrogen gas is removed. A peristaltic pump (F) directs the solution to the mass spectrometer (G) and to its ESI source. Panel **(b)** illustrates the laser plume capturing interface. The solvent is supplied through capillary (H) and forms a droplet above the laser ablation site. The laser beam is focused by a lens (J) onto the specimen from which it ablates a nano-volume of material. Some of the ablated material is electrostatically collected on the droplet surface. Upon reaching a critical size, the droplet is sheared off by the high-velocity nitrogen gas flowing into the exit capillary and transported as a coarse aerosol into the exit capillary (K), together with remaining plume material that did not attach to the droplet. Panel **(c)** shows the separatory micro-funnel. The solvent/gas mixture enters the funnel at high velocity from the exit capillary (K). In the absence of the hydrophilic surface treatment, see text, the solvent beads up and a mixture of solvent and gas is collected at the bottom of the funnel (left schematic). In contrast, with the hydrophilic treatment (right funnel), the glass surface is wetted, and a solvent film is formed on the internal walls of the funnel. Solvent is collected through the peristaltic tubing (M), and excess N_2 gas exits through the upper section of the funnel

HPLC piston pump (G4220A; Agilent, Santa Clara, CA, USA) (D) is used to provide a steady flow of a binary solvent mixture to the capturing interface (B), described in detail below. After the capturing interface, a mixture of solvent droplets, ablated material, and nitrogen gas is transported through an exit capillary to a separatory micro-funnel (E), containing less than 10 μL of solvent, in which the gas in the stream is separated from the liquid and removed. The liquid is transported though a peristaltic pump (F) into the electrospray ion source (G) of the mass spectrometer (Q-ToF, Agilent 6538).

Solvent Capturing Interface

The ablation plume capturing interface is depicted in Figure 1b. The solvent mixture (25:75 (v/v) 2-propanol:water) from the binary HPLC pump enters through the inlet capillary (H) at a flow rate of 150 μL/min. The distance between sample and end of the inlet capillary was typically 4 mm, but was increased to about 7 mm for rough samples. No change in ion signals were observed as this distance was varied. Successive hanging droplets form above the laser ablation site at the end of a 0.25 mm i.d. steel tubing. The droplet grows to a size of 1.5 to 2 mm, depending on solvent used and on the distance to the exit capillary (K in Figure 1b). Thus, at the point of droplet shear-off, the distance between sample and bottom of the droplet is typically 2 mm.

Although organic solvents are known to promote ionization in the electrospray, a relatively high surface tension is needed to form sufficiently large and stable hanging droplets; therefore, a higher water content than what is optimal for electrospray ionization (ESI) was used. The pressure of 160 Torr above atmosphere in the imaging chamber drives a flow of approximately 600 mL/min of nitrogen gas through a 1.0 mm i.d. exit tubing. The hanging droplet gradually increases in volume until the high-velocity nitrogen flow causes the droplet to shear off and disintegrate into an aerosol as it enters the exit tubing (K) together with nitrogen gas (see Supplementary Material 1). The droplet growth, disintegration,

and aerosol aspiration process repeat about three times every second.

A potential of +700 V is applied to the steel inlet capillary (H) with the sample stage grounded (see Supplementary Material 5) using a high voltage power supply (PS350; Stanford Research Systems, Sunnyvale, CA, USA). The current to the sample is recorded with a picoammeter (model 6485; Keithley, Cleveland, OH, USA).

The mixed-phase solution flows through the 2 cm-long stainless steel exit tubing (K) followed by a 1 m long, 1.0 mm i.d. polytetrafluoroethylene (PTFE) tube before reaching a laboratory-made glass micro-separatory funnel, as depicted in Figure 1c. The liquid is collected on the inside wall of the funnel and is pumped by a peristaltic pump (Sci-Q 400; Watson Marlow, Wilmington, MA, USA) through a 14 cm-long, 0.38 mm i.d., phthalate-free PVC peristaltic tubing (Spetec GmbH, Erding, Germany) connected to the ESI of the mass spectrometer. Care was taken to use phthalate-free materials throughout the system, as compounds such as dioctylphthalate may cause serious and persistent contamination of the mass spectrometer. The Agilent 6538 mass spectrometer was also employed in control experiments in which material extracted from imaged specimens was analyzed by ESI-MS in direct infusion experiments.

The glass micro-separatory funnels were drawn from disposable glass Pasteur pipettes. In order to minimize solvent dispersion in the device, its volume was made as small as practical. In initial experiments, the surface tension of the solvent caused the liquid to bead up on the inner glass walls of the funnel (Figure 1c, left image), stopping the flow and promoting mixing (peak broadening). To counteract this, the funnel is heat-treated in the flame of a Bunsen burner to 400°C (as evidenced by a yellow sodium flame) to induce hydrophilicity [23]. After treatment, the flowing liquid forms a film on the inner glass surfaces, which allows the solvent to flow evenly down the funnel (Figure 1c, right image). The hydrophilic effect lasted for about 10 h of operation, and the funnel was heat-treated prior to each imaging experiment.

In order to minimize mixing after the peristaltic pump, the flow rate was adjusted to be slightly higher than that of the solvent supply. As a result, the solvent flowing into the peristaltic pump was separated by "plugs" of nitrogen gas, typically produced at a rate of 1 per s, but occasionally in a range of 2 to 0.20 per s. Such separation of the solvent is known to reduce the mixing that normally occurs when liquid flows through a pump or a capillary [24]. After the peristaltic pump, the pressure in the tubing was approximately 6 atm, and the volume of each gas bubble was about 5% of the volume of each liquid "plug." Upon reaching the electrospray nebulizer, the gas was depressurized and expelled within approximately 50 to 100 ms, during which time the ion signal was diminished. The effect on the abundance measurement is estimated to be less than 2% in almost all cases and much smaller than other sources of abundance errors. Indeed, no effect of the gas bubbles on relative abundances could be detected.

Imaging Procedure

The mid-IR laser light at 2.94 μm is selected to coincide with the maximum of an absorption band of liquid water, and it is therefore required that the sample remains hydrated in order to achieve consistent and effective ablation throughout the length of the typical imaging experiment (i.e., during a time period ranging from 1 to 6 hours. To limit water loss, the sample is cooled to a temperature of 0 to –10°C, depending on sample sensitivity to freezing. For each pixel in the image, a 1-s-long sequence of twenty 2.94 μm laser pulses of 1.5 mJ each is focused onto the same spot on the sample. The size of the laser focus is approximately 220×260 μm. The ablation depth for a well-hydrated biological sample is about 10-25 μm; thus the ablated volume in each pixel is approximately 1 nL. Part of the material in the laser plume is collected on the surface of the hanging droplet, with the assistance of the applied potential, and the remaining plume material is aspirated into the collection capillary. Owing to the rapid turnover of capturing droplets, the ablated material from each pixel is distributed amongst three to five successive droplets (see Supplementary Material 6). With a solvent flow rate of 150 μL/min, 1 nL of sample is diluted into 2.5 μL of solvent, resulting in a dilution ratio (v/v) of 1:2500. An approximately 5-fold additional dilution occurs in the tubing leading to the ion source.

During image acquisition, in-house software controls the firing of the laser and the motion of the XYZ-stage. The software also records XYZ-stage locations and time. A second computer controls the QToF mass spectrometer and records two mass spectra per s throughout the imaging experiment. Each mass spectrum is internally mass calibrated using two peaks at m/z 121.0509 and 922.0098, provided by electrospraying a reference solution using a second nebulizer. After completed data acquisition, additional in-house software matches individual pixels with the mass spectra (usually 4–8) recorded as the analytes sampled from the pixel reach the ion source (see also Supplementary Information 11). For any m/z value, the sum of the abundances recorded in the selected mass spectra is used for image construction. Additional software generates images for high mass resolution features or, alternatively, for specified mass ranges, and performs image analysis to find, for example, sets of selected ions with similar spatial distributions (co-spatial ions). The visual images presented in this report were produced by the GIMP graphics program. In scaling the MS images to the higher resolution printed images, the experimental ion peak abundance value measured in each MS imaging pixel is assigned to the center of the pixel location. Abundance values at intermediate locations were obtained by (bicubic) interpolation. For any selected ion, the range of abundance values were normalized to a scale of 0 to 100, and the latter values were color-coded as shown by the linear color bar on each image.

Chemicals

Amino acid standards (Sigma-Aldrich, 98% pure by TLC) were used without further purification. Solvents, including

water, were of HPLC grade (Sigma-Aldrich). Agar plates were prepared using LB Agar Miller (DIFCO Microbiology, Lawrence, KS, USA).

Amino Acid-Infused Agar Plates

An imaging test pattern consisting of small circular areas of amino acid-infused solidified agar surrounded by unaltered (control) agar was prepared as follows. Phenylalanine, lysine, tryptophan, and arginine were selected as amino acid standards and prepared as individual 20 mL volume aqueous 0.10 M solutions. Agar powder was added to these solutions according to manufacturer instructions to a final concentration of 20% (w/v). The solutions were heated to the boiling point, poured into separate sterile Petri dishes and allowed to solidify at 21°C. Circular discs (5 mm diameter) were cut out from each of the four amino acid-infused agar plates. Four discs of the same size were cut out from a control (amino-acid free) agar plate in a square lattice pattern, removed and discarded. The four amino acid-infused agar discs were carefully fitted into the vacant spaces on the control agar plate. Diffusion of small molecules in agar is relatively fast; therefore, to limit lateral diffusion of amino acids and other compounds over test pattern boundaries, plates were frozen at –10°C within 20 min of being assembled and processed within 1 h. Imaging over 25 × 30 pixels was performed with 20 laser shots per pixel.

Plant Material

A cultivated species of *Alstroemeria* (Peruvian Lily, similar to *Alstroemeria stakaros* [25]) and red radish (*Raphanus sativus* L.) were purchased from a local grocery store in Norman, OK, USA. A single flower petal and one globular radish taproot with a remnant green basal rosette section were selected for LASCA imaging. Prior to imaging, both the petal and the taproot were rinsed with nanopure water. A longitudinal section was cut from the red radish taproot, using a 70% (v/v) alcohol-cleaned razor blade. Each specimen was placed on the LASCA stage and imaged separately.

Results and Discussion

Performance of the MSI System

The design considerations for the present LASCA interface are best understood from the problems encountered with the preceding versions of the laser-ablation, plume-capturing interface, and this needs to be addressed here in some detail. In an early version of the interface, a continuous flow of solvent was used in the form of a "liquid bridge" suspended by surface tension between two opposing capillary butt ends, separated by 2–3 mm [16, 17]. As discussed in the Introduction, the problem of the low efficiency of capture of ablated analytes [12, 15] was solved by applying a high voltage between the laser ablation site and the liquid bridge [16, 17]. The main remaining issue was that while the rise in analyte MS signal was rapid after the 1-s-long laser ablation period, its decay was much slower, with

a half-life of about 15 s. The resulting peak-broadening constituted a serious problem, as it decreased sensitivity and slowed image acquisition.

It was determined that analyte peak broadening was chiefly due to slow analyte/solvent mixing in the liquid bridge. First, as the diameter of the bridge is much larger than the i.d. of either of the two capillaries, the velocity distribution in a cross section of the liquid bridge was uneven, with the fastest flow along the centerline of the cylindrical bridge and a much slower flow in the near-surface. As the plume material is initially incorporated into the surface layers of the solvent bridge, the analyte peak width is determined by the rate of diffusion of analytes into the inner higher-velocity volumes. Analyte removal from the bridge is particularly slow for hydrophobic materials (such as lipids) that tend to accumulate and remain on liquid surfaces. Such surface accumulation could be observed by the naked eye. In addition to slow mixing in the liquid bridge, analyte adsorption on the interior walls of the capillary leading to the electrospray source also contributed to the observed slow analyte signal decay.

The LASCA interface was purposefully designed to overcome the problem of slow analyte mixing into the liquid flow. In order to force laser-ablated analytes collected on a solvent surface to enter the collection capillary, the "flying droplet" interface, depicted in Figure 1b, was invented. As already stated, hanging droplets are repeatedly formed, detached, and captured by the exit capillary. Since the surface of the hanging droplet is sheared off during this process, the slow transport rate of surface active analytes into the bulk of the solvent is no longer a limiting factor for achieving narrow peak widths.

The time dependence of selected ion signals in the "flying droplet" interface was studied in separate experiments (for details see Supplementary Material 8). Briefly, it was found that after a pixel location had been sampled using a 1-s-long sequence of 20 laser pulses and maximum ESI signal obtained, the ion signals decayed roughly exponentially. The half-life was about 7 s if the solution stream was not separated with gas bubbles, and about 4 s if gas bubbles were used. The decay time and, thus, pixel peak widths showed minimal variation between analytes, but did vary with solvent composition. For example, when a binary isopropanol/water solvent mixture was used, peaks widened with increasing isopropanol content and narrowed with increasing water content.

Owing to peak broadening, the signal of any selected ion observed while sampling at a given location (pixel) contains contributions from previously sampled locations. With ion signal decay half-lives of about 4 s, images could be recorded at a rate of 10 pixels per min, with negligible carry-over from one pixel to the next. Thus, a 1000 pixel image can be obtained in about 1 and 3/4 h. Faster image recording rates are clearly possible, especially with the use of an in-house developed numerical procedure by which overlapping ion signals from adjacent pixels are deconvoluted and assigned to their respective pixels (see Supplementary Material 8). At a given recording rate, the deconvolution procedure yields more accurate

abundance values for each pixel and improves the spatial resolution.

The LASCA platform is coupled to a high resolution, Q-ToF mass spectrometer (HRMS).The use of HRMS is paramount to the targeted application of imaging metabolomics from complex specimens, such as plant, animal, or human tissues and/or microbial biofilms, as it allows for the detection and imaging of a large number of different metabolites [9]. This is illustrated for LASCA imaging in Figure 2, which shows a 310 mDa range, from m/z 477.06 to 477.37, of a mass spectrum obtained by summing over all pixels in an image of test pattern of amino acid infused agars, see next section. The mass resolution in the spectrum in Figure 2 is about 35,000 at half-height. Seven peaks are seen to be clearly resolved, and the insets demonstrate that the images obtained for each of these are all unique and different. If a unit mass-resolution MS had been used for this work, the selected ion image obtained at m/z 477 would have represented the sum of these seven different images. Clearly, such composite images would make any detailed chemical analysis of a complex sample nearly impossible. Figure 2 further demonstrates that useful images can be obtained even for very low-abundance ions.

Imaging Results

The performance of the LASCA system was evaluated by imaging a test pattern of amino acid-infused agar plugs (Figure 3a). In imaging mode, the method of introducing gas bubbles into the solvent stream to the MS was used and the decay half-life decreased to 3.8 s (see Supplementary Material 9). The pixels were separated by 12 s. Chromatograms and mass spectra showing the data quality are available in Supplementary Materials 10–12. Selected ion images were generated from the data for several thousand different m/z peaks. The manual inspection of images was restricted to the most abundant 2300 ions. Of these, images for 1265 selected ions displayed a distinct pattern. The large majority of those ions originated from only one of the four amino acid-infused agar discs. Identification of the major ions is provided in Supplementary Material 13.

Images of an additional 1000 "background" ions displayed no meaningful spatial heterogeneity. These originated either from the agar or were present as background or contaminants in the imaging system (e.g., in the solvents, in polymers, and other materials in contact with the solvents, or in the ion source). The two groups of ions are easily distinguished by the fact that the abundances of agar-related ions correlate with the laser being turned on and off, whereas the abundances of contaminant or background ions do not. Finally, it should be noted that a significant number of ions, of all categories, are due to cluster formation between ions and neutrals in the ionization process. For example, a
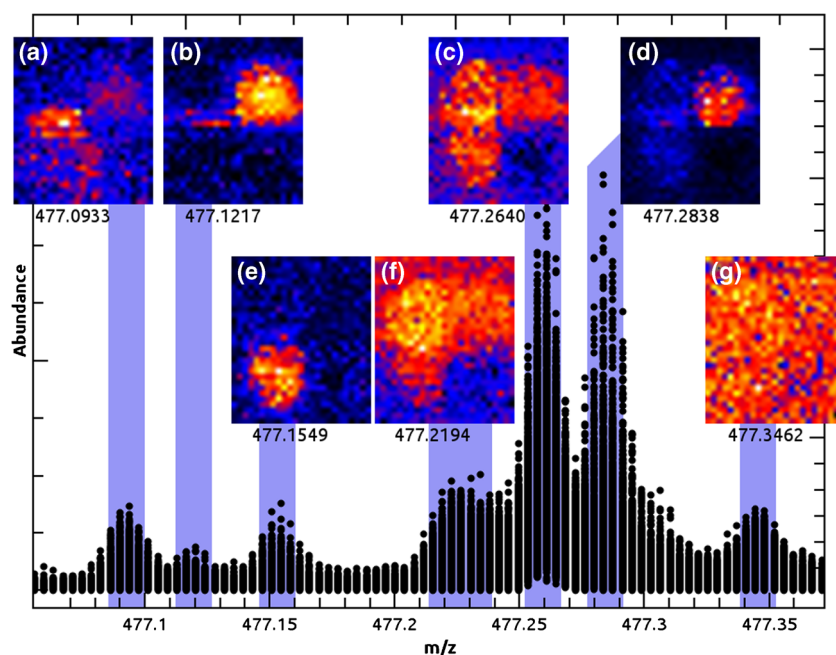

Figure 2. Representative high-mass resolution mass spectrum of amino acid-infused agar plate (c.f. Figure 3) around integral m/z value of 477. The insets show LASCA images (25 × 30 pixels) associated with each of the seven different ions identified in the mass spectrum, revealing strikingly different spatial distributions for ions with the same integral m/z value. The mass spectrum was acquired by overlaying the mass spectra obtained for all 750 pixels, each of which consists of seven spectra collected over a 3.5 s time period of maximum laser-ablation derived ion signals (i.e., from a total of 5250 mass spectra and about 440,000 individual abundance values). Ions with a measured mass within ±15 ppm (equivalent to ±7 mDa) of the respective peak centroid were used for image construction
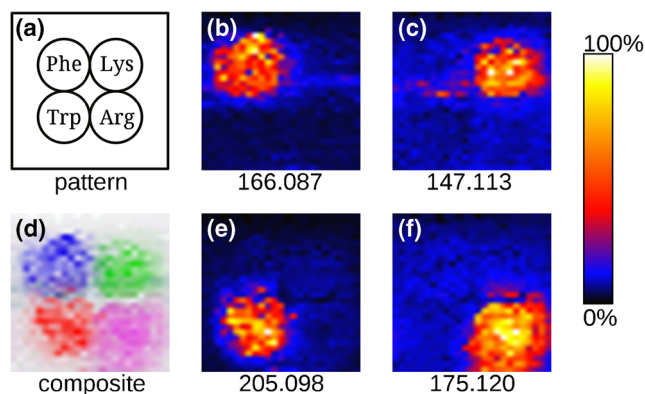
Figure 3. LASCA imaging of an amino acid test pattern. Each image contains 25 × 30 pixels over a 20 × 20 mm square area. Individual panels represent: **(a)** test specimen consisting of four 5-mm-diameter plugs, each infused with a different amino acid and surrounded by unaltered agar; **(d)** composite, false-color image constructed from the LASCA-MSI images presented in panels **(b)**, **(c)**, **(e)** and **(f)** showing the locations of each of the four amino acids. The latter panels depict individual images obtained for protonated forms of **(b)** phenylalanine at *m/z* 166.087; **(e)** tryptophan at *m/z* 205.098; **(c)** lysine at *m/z* 147.113; and **(f)** arginine at *m/z* 175.120. The maximum mass error allowed for each selected ion image was ±20 ppm. For each image in **(b)**, **(c)**, **(e)** and **(f)**, the abundances of the selected ion are normalized to set the minimum and maximum to 0 and 100%, respectively

cluster ion of a sample-generated ion with a molecule present in the background will show the spatial distribution of the former.

The images of the primary amino acid peaks (Figure 3b, c, e, and f) show that they are detected solely in the area of the agar plugs into which they were incorporated, as expected. A composite false-color image for these four ions is shown in Figure 3d. Laboratory-designed software was used to mine the data for images that showed the same spatial patterns as any one of the four amino acid ions, and 200–400 distinct ions were found to be uniquely associated with each. Additional ions were observed from two of more of the amino acid regions, and they represent common amino acid ionic fragments.

A few ions yielded more complex images, as illustrated in Figure 2. Two to six ions were observed from each of the four border regions, where two different amino acid-infused agars were in contact with each other. For example, the peak at *m/z* 477.0933 was detected primarily in the border region between the phenylalanine and tryptophan-doped agars. Ions observed in border regions were found to represent mixed clusters between the two amino acids. Moreover, the peak at *m/z* 477.2640, while observed from agar doped with phenylalanine, lysine, or tryptophan, was absent from arginine-doped agar. No evidence of any chemical reactions was found.

A section from each of the four amino acid-infused agars was subjected to a standard extraction procedure and analyzed with Q-ToF mass spectrometry by direct infusion. In each case, the mass spectra obtained in imaging mode closely matched the spectra obtained using extraction and direct infusion (data not shown). This demonstrates that any laser-induced molecular damage, if at all present, was negligible.

With regard to LASCA sensitivity, it was determined that the volume of agar ablated in each pixel was approximately 1 nL, containing 100 pmol of an amino acid standard, and that the base peak (i.e., the protonated amino acid) had an S/N ratio of approximately 3000.

The LASCA imaging system was further tested using two different plant specimens, a flower petal and a red radish taproot (Figures 4 and 5, respectively). Leaves and flower petals have been employed by a number of investigators to demonstrate the performance of novel ambient MSI techniques [26–30]. Photographs of the *Alstromeria* spp. flower petal, prior to and after LASCA imaging, as well as selected LASCA images of the petal, are presented in Figure 4a–j. The areas of laser beam ablation are seen as circular punctures (Figure 4b). A total of 3160 features were detected in this petal image. Some features displayed a nearly homogeneous distribution over the entire imaged area. Obvious heterogeneity was, however, displayed for about 200 ions. The abundance distributions of many of these ions correlate with the distribution of the yellow and pink pigments. A selection of eight LASCA images is presented in Figure 4c–j. The mass peak at *m/z* 595.2 (Figure 4e) was identified with cyanidin 3-rutinoside (antirrhinin), which is a pigment commonly found in many species of *Alstroemeria* [31]. Other mass peaks remain unassigned.

An optical image and several LASCA images of the upper part of the radish taproot section are presented in Figure 5a and in Figure 5b–n, respectively. Approximately 2000 selected ion images were obtained, demonstrating a large variety of different spatial distributions. Certain ions are preferentially formed from areas that contain the dark-red surface pigment (Figure 5m, n, j), whereas other ions are associated with a white flesh of the taproot (Figure 5b, k, g) or with green stem sections of a basal rosette (Figure 5c, d, e, f, h). Several ions are present in multiple areas (Figure 5i). The peak at *m/z* 271.060 ($C_{15}H_{11}O_5^+$) is identified with pelargonidin (Figure 5m) [32]. Its detection is confined to the zone characterized by the dark red pigment seen in Figure 5a. Additional 90 LASCA images obtained from the radish taproot, including glycosylated derivatives of pelargonidin detected as *m/z* 903.252 and 933.265 [32, 33], are available in Supplementary Material 14.

LASCA MSI has also been applied to imaging of bacterial colonies cultivated on nutrient agar (see Supplementary Material 7). Imaging of biofilms on surfaces of corroding metals have been reported elsewhere [22].
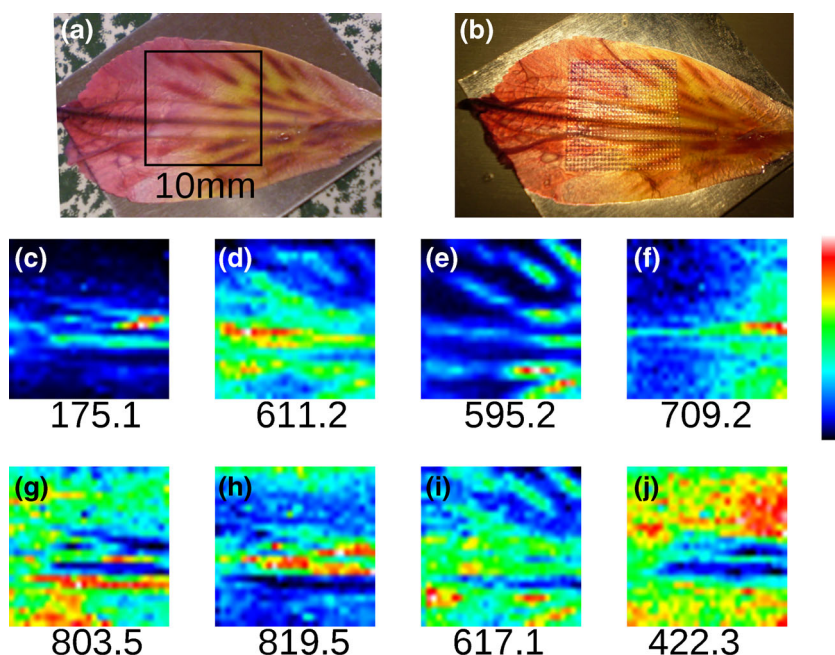
Figure 4. Photographs **(a)**, **(b)** and LASCA images **(c)**–**(j)** of an *Alstroemeria* spp. (Peruvian lily) flower petal. Photographic images of petal **(a)** prior to and **(b)** following LASCA imaging. Lower panel presents eight selected ion images to demonstrate different types of spatial distribution patterns of chemical compounds. In **(e)**, the ion producing the peak at *m/z* 595.166 **(e)**, is identified with $C_{27}H_{31}O_{15}^{+}$, cyanidin 3-rutinoside (antirrhinin), which is a common plant pigment
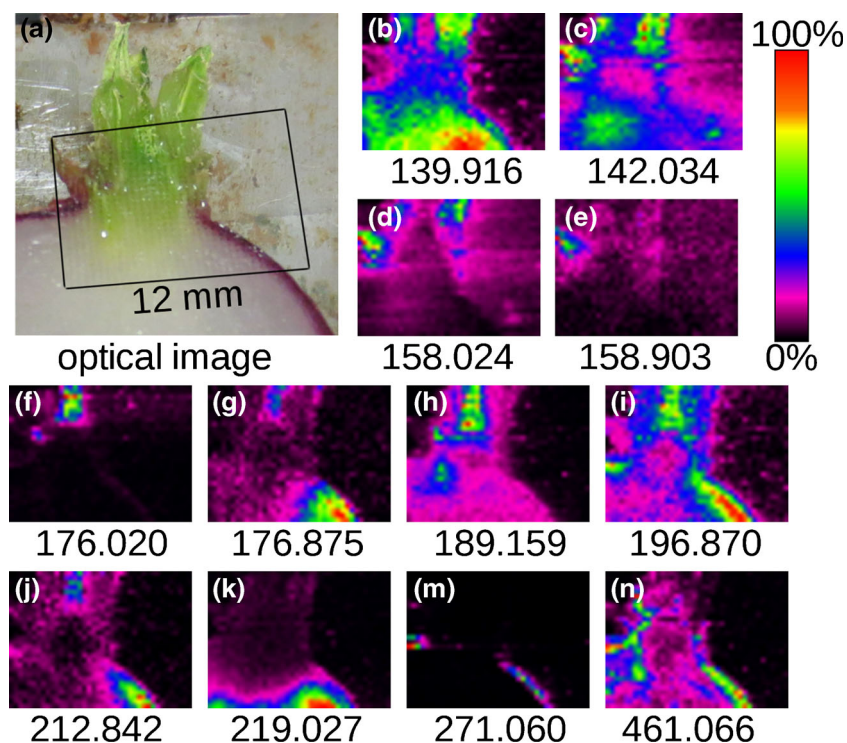

Figure 5. Optical **(a)** and 40 × 30 pixel LASCA images **(b)**–**(n)** of a longitudinal section of a red radish taproot with a green rosette stem part. The ion producing the peak at *m/z* 271.060 **(m)**, which is unique to a red-colored area in **(a)** is identified with the pigment pelargonidin

Conclusions

The design of the LASCA system allows for significant flexibility in terms of (1) locating the (often bulky) mass spectrometer relative to the imaging equipment, (2) choice of ionization and detection method, and (3) possible application of various real-time sample preparation procedures, such as extractions or chromatography. The LASCA platform facilitates imaging of a broad range of materials, such as as-received biological samples, including living biofilms and plant specimens, with varying size and surface topography. Although not demonstrated here, LASCA MS can employ a wide range of laser wavelengths to achieve metabolomic imaging.

The efficient sampling of laser-generated plumes, combined with electrospray ionization and a high mass resolution mass spectrometry, allows the detection of a large number of compounds, up to about 2000, from a single pixel. Thus, LASCA-MS system enables meaningful statistical analysis of imaging metabolomics, even in the absence of chromatography.

The LASCA platform offers a plethora of applications in life science fields, including medical, environmental, drinking water, food, and pharmaceutical research. Importantly, it opens up a possibility of not only metabolomic imaging of inanimate specimens but also of temporal, including real-time, and spatial (i.e., in three dimensions) characterization of metabolomic activities in highly complex, living biological systems.

Acknowledgments

References

1. Wu, C., Dill, A.L., Eberlin, L.S., Cooks, R.G., Ifa, D.R.: Mass spectrometry imaging under ambient conditions. Mass Spectrom. Rev. **32**, 218–243 (2013)
2. Caprioli, R.M., Farmer, T.B., Gile, J.: Molecular imaging of biological samples: localization of peptides and proteins using MALDI-TOF MS. Anal. Chem. **69**, 4751–4760 (1997)
3. Shiea, J., Huang, M.Z., Hsu, H.J., Lee, C.Y., Yuan, C.H., Beech, I., Sunner, J.: Electrospray-assisted laser desorption/ionization mass spectrometry for direct ambient analysis of solids. Rapid Commun. Mass Spectrom. **19**, 3701–3704 (2005)
4. Nemes, P., Barton, A.A., Li, Y., Vertes, A.: Ambient molecular imaging and depth profiling of live tissue by infrared laser ablation electrospray ionization mass spectrometry. Anal. Chem. **80**, 4575–4582 (2008)
5. Nemes, P., Vertes, A.: Laser ablation electrospray ionization for atmospheric pressure, in vivo, and imaging mass spectrometry. Anal. Chem. **79**, 8098–8106 (2007)
6. Sampson, J.S., Hawkridge, A.M., Muddiman, D.C.: Generation and detection of multiply-charged peptides and proteins by matrix-assisted laser desorption electrospray ionization (MALDESI) Fourier transform ion cyclotron resonance mass spectrometry. J. Am. Soc. Mass Spectrom. **17**, 1712–1716 (2006)
7. Rezenom, Y.H., Dong, J., Murray, K.K.: Infrared laser-assisted desorption electrospray ionization mass spectrometry. Analyst **133**, 226–232 (2008)
8. Shrestha, B., Nemes, P., Vertes, A.: Ablation and analysis of small cell populations and single cells by consecutive laser pulses. Appl. Phys. A **101**, 121–126 (2010)
9. Bereman, M.S., Nyadong, L., Fernandez, F.M., Muddiman, D.C.: Direct high-resolution peptide and protein analysis by desorption electrospray ionization Fourier transform ion cyclotron resonance mass spectrometry. Rapid Commun. Mass Spectrom. **20**, 3409–3411 (2006)
10. Huang, M.Z., Jhang, S.S., Cheng, C.N., Cheng, S.C., Shiea, J.: Effects of matrix, electrospray solution, and laser light on the desorption and ionization mechanisms in electrospray-assisted laser desorption ionization mass spectrometry. Analyst **135**, 759–766 (2010)
11. Ovchinnikova, O.S., Kertesz, V., Van Berkel, G.J.: Combining transmission geometry laser ablation and a non-contact continuous flow surface sampling probe/electrospray emitter for mass spectrometry based chemical imaging. Rapid Commun. Mass Spectrom. **25**, 3735–3740 (2011)
12. Park, S.G., Murray, K.K.: Infrared laser ablation sample transfer for MALDI and electrospray. J. Am. Soc. Mass Spectrom. **22**, 1352–1362 (2011)
13. Ovchinnikova, O.S., Kertesz, V., Van Berkel, G.J.: Combining laser ablation/liquid phase collection surface sampling and high-performance liquid chromatography-electrospray ionization-mass spectrometry. Anal. Chem. **83**, 1874–1878 (2011)
14. Lorenz, M., Ovchinnikova, O.S., Van Berkel, G.J.: Fully automated laser ablation liquid capture surface analysis using nanoelectrospray ionization mass spectrometry. Rapid Commun. Mass Spectrom. **28**, 1312–1320 (2014)
15. Park, S.G., Murray, K.K.: Infrared laser ablation sample transfer for on-line liquid chromatography electrospray ionization mass spectrometry. J. Mass Spectrom. **47**, 1322–1326 (2012)
16. Kaufman, E., Smith, W., Kowalski, M., Beech, I., Sunner, J.: Electric-field-enhanced collection of laser-ablated materials onto a solvent bridge for electrospray ionization mass spectrometry. Rapid Commun. Mass Spectrom. **27**, 1567–1572 (2013)
17. Kaufman, E., Sunner, J.: Ambient laser ablation/solvent flow bridge capture of analytes for ESI-MS and imaging of living biofilms. Proceedings of the 60th Annual ASMS Conference on Mass Spectrometry and Allied Topics. Vancouver, 20–24 May (2012)
18. Park, S.-G., Murray, K.K.: Ambient laser ablation sampling for capillary electrophoresis mass spectrometry. Rapid Commun. Mass Spectrom. **27**, 1673–1680 (2013)
19. Apitz, I., Vogel, A.: Material ejection in nanosecond Er: YAG laser ablation of water, liver, and skin. Appl. Phys. A **81**, 329–338 (2005)
20. Brauer, J.I., Beech, I., Kaufman, E., Sunner, J.: Mass spectrometry imaging of biological systems using laser ablation and solvent plume arrest (MSI-LASPA). Proceedings of the 62nd ASMS Conference on Mass Spectrometry and Allied Topics. Baltimore, 15–19 June (2014)
21. Brauer, J.I., Smith, W., Sunner, J.: Imaging of biological systems using laser ablation and a "flying droplet" interface for analyte capture. Proceedings of the 61st Conference on Mass Spectrometry and Allied Topics. Minneapolis, 9–13 June (2013)
22. Brauer, J.I., Makama, Z., Bonifay, V., Aydin, E., Kaufman, E., Beech, I.B., Sunner, J.: Mass spectrometric metabolomic imaging of biofilms on corroding steel surfaces using laser ablation and solvent capture by aspiration. Biointerfaces **10**, 019003 (2015)
23. Laskowsk, J., Kitchene, J.A.: The hydrophilic—hydrophobic transition on silica. J. Colloid Interface Sci. **29**, 670 (1969)
24. Skeggs, L.T.: An automated method for colorimetric analysis. Am. J. Clin. Pathol. **28**, 311–322 (1957)
25. van Andel, J.: Alstroemeiria named Stakaros. US Plant Patent 5133 (1983)
26. Li, Y., Shrestha, B., Vertes, A.: Atmospheric pressure infrared MALDI imaging mass spectrometry for plant metabolomics. Anal. Chem. **80**, 407–420 (2008)
27. Perdian, D.C., Schieffer, G.M., Houk, R.S.: Atmospheric pressure laser desorption/ionization of plant metabolites and plant tissue using colloidal graphite. Rapid Commun. Mass Spectrom. **24**, 397–402 (2010)
28. Nemes, P., Barton, A.A., Vertes, A.: Three-dimensional imaging of metabolites in tissues under ambient conditions by laser ablation electrospray ionization mass spectrometry. Anal. Chem. **81**, 6668–6675 (2009)

29. Li, B., Hansen, S.H., Janfelt, C.: Direct imaging of plant metabolites in leaves and petals by desorption electrospray ionization mass spectrometry. Int. J. Mass Spectrom. **348**, 15–22 (2013)

30. Cha, S., Zhang, H., Ilarslan, H.I., Wurtele, E.S., Brachova, L., Nikolau, B.J., Yeung, E.S.: Direct profiling and imaging of plant metabolites in intact tissues by using colloidal graphite-assisted laser desorption ionization mass spectrometry. Plant J. **55**, 348–360 (2008)

31. Nørbaek, R., Christensen, L.P., Bojesen, G., Brandt, K.: Anthocyanins in Chilean species of *Alstroemeria*. Phytochemistry **42**, 97–100 (1996)

32. Giusti, M.M., Wrolstad, R.E.: Characterization of red radish anthocyanins. J. Food Sci. **61**, 322–326 (1996)

33. Otsuki, T., Matsufuji, H., Takeda, M., Toyoda, M., Goda, Y.: Acylated anthocyanins from red radish (*Raphanus sativus* L.). Phytochemistry **60**, 79–87 (2002)